clean technologies

Article

Design-of-Experiments Analysis of Green Methanol Oxidative Reforming over Agglomerated Catalysts for Hydrogen Production

Pedro J. Megía [1,*], Álvaro Moreno de la Calle [1,2], Arturo J. Vizcaíno [1], José A. Calles [1,2] and Alicia Carrero [1,2]

[1] Chemical and Environmental Engineering Group, Universidad Rey Juan Carlos, c/Tulipán s/n, 28933 Móstoles, Spain; alvaro.moreno@urjc.es (Á.M.d.l.C.); arturo.vizcaino@urjc.es (A.J.V.); joseantonio.calles@urjc.es (J.A.C.); alicia.carrero@urjc.es (A.C.)
[2] Instituto de Investigación de Tecnologías para la Sostenibilidad, Universidad Rey Juan Carlos, c/Tulipán s/n, 28933 Móstoles, Spain
* Correspondence: pedro.megia@urjc.es

Abstract

In this work, sustainable hydrogen production from green methanol via oxidative reforming was investigated over agglomerated Co-Cr/SBA-15 catalysts. A mixed factorial design of experiments was applied to the effects of temperature, weight hourly space velocity (WHSV), steam-to-carbon ratio (S/C), and oxygen-to-carbon ratio (O_2/C) on methanol conversion and hydrogen yield. The developed models exhibited good predictive performance within the investigated operating domain. Temperature and WHSV were identified as the most influential variables for both responses, whereas increasing the S/C ratio significantly enhanced hydrogen yield. In contrast, higher O_2/C ratios promoted methanol conversion, but reduced hydrogen yield due to enhanced oxidation pathways. Optimal conditions for hydrogen production were identified at 600 °C, WHSV= 30 h^{-1}, S/C = 2, and O_2/C = 0.10. Under these conditions, the agglomerated catalyst showed catalytic performance comparable to that of the powdered counterpart, confirming that shaping with bentonite does not compromise activity. Furthermore, the shaped catalyst retained approximately 95% of its initial methanol conversion after 50 h time-on-stream while maintaining an almost constant hydrogen yield, with negligible coke formation and cobalt sintering. These results demonstrate the potential of agglomerated Co-Cr/SBA-15 catalysts for hydrogen production from green methanol under the investigated oxidative steam reforming conditions and stable performance over 50 h time-on-stream.

Keywords: renewable hydrogen; green methanol; Co-Cr/SBA-15 catalysts; shaped catalysts; experimental design

Check for updates

Academic Editor: Denitza Zgureva

Received: 23 September 2026
Revised: 19 October 2026
Accepted: 22 October 2026
Published: 26 October 2026

Copyright: © 2026 by the authors. Licensee MDPI, Basel, Switzerland. This article is an open access article distributed under the terms and conditions of the Creative Commons Attribution (CC BY) license.

1. Introduction

Since the global energy supply remains predominantly dependent on fossil fuels [1], the development of sustainable energy carriers has become a research priority. Among the different energy applications, hydrogen has emerged as a promising energy carrier for fuel cell electric vehicles, especially in heavy-duty transport sectors, where the weight and volume of batteries required for long-range operation can limit the viability of fully battery-electric solutions [2]. This growing interest is driving efforts to design systems capable of storing and transporting hydrogen in a safe and efficient manner [3]. In this context, liquid organic hydrogen carriers (LOHCs) are gaining increasing attention, with

methanol emerging as a promising candidate due to its high energy density, ease of storage and transport, and potential to contribute to a lower carbon footprint [4,5]. However, the environmental impact of methanol is linked to its production pathway. Methanol derived from fossil fuels has a high carbon footprint which limits its suitability as an energy carrier in a climate-neutral scenario. Therefore, producing green methanol has become essential for its use in sustainable energy systems [6]. Green methanol is typically produced from syngas derived from lignocellulosic biomass through three main steps: (i) biomass gasification to generate syngas, (ii) syngas cleaning and conditioning, and (iii) catalytic conversion of syngas into methanol [7,8]. Nevertheless, while this renewable feedstock may contribute to reducing the carbon footprint associated with hydrogen production, the overall environmental performance of the process also depends on additional factors such as process energy requirements, oxygen consumption, catalyst lifetime, and downstream hydrogen purification requirements. Catalytic conversion processes based on reforming pathways have attracted significant attention due to their high hydrogen yields [9,10]. These processes involve several concurrent reactions, including methanol steam reforming (Equation (1)), thermal decomposition (Equation (2)), and the water–gas shift reaction (Equation (3)) [11,12].

$$CH_3OH + H_2O \leftrightarrow 3H_2 + CO_2;\ \Delta H > 0 \quad (1)$$

$$CH_3OH \leftrightarrow 2H_2 + CO;\ \Delta H > 0 \quad (2)$$

$$CO + H_2O \leftrightarrow H_2 + CO_2;\ \Delta H < 0 \quad (3)$$

The main drawback of steam reforming is its high energy demand. The co-feeding of oxygen introduces exothermic oxidation pathways that can partially compensate for the energy demand of endothermic reactions, improving the overall thermal efficiency of the process [13]. A schematic representation of the main reaction pathways associated with oxidative steam reforming of methanol is shown in Figure 1.

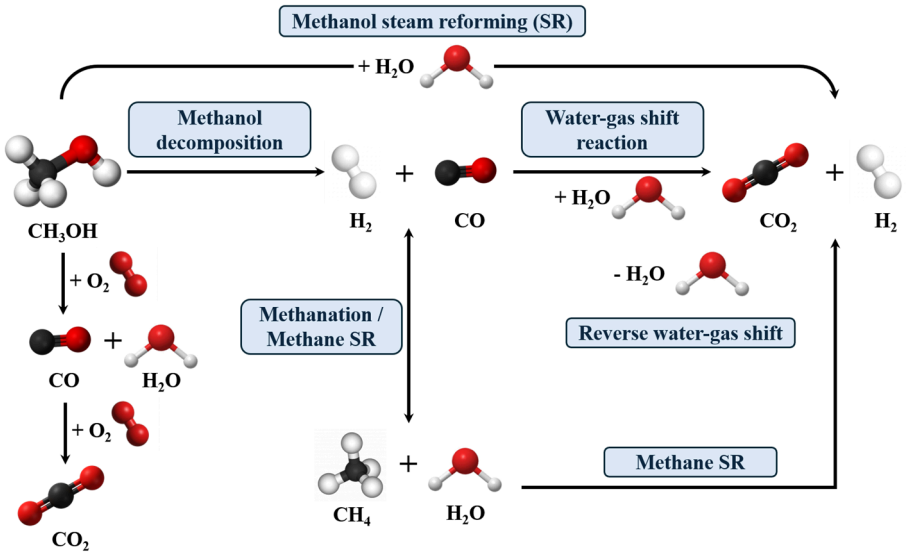


Figure 1. Schematic representation of the main reaction pathways involved in the oxidative steam reforming of methanol.

As a catalytic process, oxidative steam reforming requires the development of suitable catalysts since they directly affect both the methanol conversion and the selectivity toward the desired products. In this regard, SBA-15 has been widely used as a catalyst support owing to its ordered mesostructure, high surface area, and well-defined pore system.

These textural characteristics promote the homogeneous dispersion of active species while facilitating mass transport during the reaction [14–16]. Among the active phases explored for the catalytic upgrading of oxygenated compounds, cobalt has demonstrated remarkable performance in the reforming of ethanol [17], acetic acid [18,19], glycerol [20,21] and furfural [22,23]. However, its application to methanol-to-hydrogen conversion has received comparatively less attention, despite its capacity to activate both C-H and O-H bonds and its high activity toward the water–gas shift reaction. To improve the performance of Co-based catalysts, several approaches have been investigated, including the design of bimetallic systems. In this context, we previously demonstrated that the incorporation of Cr into Co-based catalysts enhances cobalt dispersion and, consequently, catalytic performance during acetic acid steam reforming [14]. Despite these advances, most reforming catalysts are still prepared as fine powders. Although powder catalysts are well suited for fundamental and kinetic studies, their implementation in fixed-bed reactors at larger scales is limited by the excessive pressure drop associated with their small particle size [24,25]. At larger scales, catalysts are typically shaped into larger and mechanically robust structures to prevent excessive pressure drop in fixed-bed reactors. Among the available shaping methods, extrusion is generally preferred for fixed-bed reactors because it is cost-effective and helps preserve the surface area and porosity of the catalyst [26,27]. The resulting structures—commonly cylindrical or ring-shaped extrudates—are obtained by incorporating inorganic binders into the catalyst formulation. Bentonite has attracted considerable attention as a shaping binder owing to its widespread availability, low cost, and high plasticity, which make it particularly suitable for extrusion-based catalyst shaping [28]. Furthermore, it has been reported to provide enhanced mechanical strength compared with other commonly used clay-based binders, such as attapulgite and sepiolite [29], while maintaining suitable textural properties for catalytic applications. Despite these advances, limited information is available regarding the combined influence of catalyst shaping and operating conditions on the performance of Co-Cr/SBA-15 catalysts during methanol oxidative steam reforming. Furthermore, comprehensive studies capable of simultaneously evaluating the effects and interactions of the main operating variables remain scarce.

Based on the above, this work investigates hydrogen production from green methanol under oxidative steam reforming conditions over bentonite-agglomerated Co-Cr/SBA-15 catalysts. The study combines catalyst shaping with a statistical design-of-experiments approach to evaluate the influence of the main operating variables on hydrogen production. Compared with conventional one-factor-at-a-time approaches, this strategy provides a more comprehensive understanding of the process and enables the identification of optimal operating conditions. By simultaneously addressing catalyst shaping and operating-condition evaluation, the present work contributes to filling this gap through the systematic assessment of a shaped Co-Cr/SBA-15 catalyst under fixed-bed operation. The results offer insight into the role of operating conditions in hydrogen production and demonstrate the potential of shaped Co-Cr-based catalysts for efficient catalytic conversion of green methanol under oxidative steam reforming conditions.

2. Materials and Methods

A more detailed description of the catalyst synthesis and extrusion procedure can be found elsewhere [14,24]. Broadly, the Co-Cr/SBA-15 catalyst in powder form was synthesized through wetness co-impregnation using an aqueous solution of the corresponding nitrates to get 7 wt.% and 2 wt.% of Co and Cr (Sigma-Aldrich, St. Louis, MO, USA), respectively, using SBA-15 as the support. The extruded catalysts were subsequently prepared by mixing the powdered catalyst with bentonite (Thermo Scientific, Waltham, MA, USA) as an inorganic binder and methylcellulose (Sigma-Aldrich), to improve paste viscosity.

After adding deionized water, the mixture was homogenized into a workable paste and conditioned in a humid environment to improve its plasticity. The paste was then extruded through a hand-made extruder equipped with a circular die and cut into cylindrical pellets (25 mm length). These pellets were dried at 110 °C and later calcined at 650 °C to remove organic components and stabilize the final structure.

The catalyst was characterized to assess its physicochemical properties and reducibility through ICP-OES, N_2 physisorption, and H_2-TPR analyses. Elemental composition was quantified through inductively coupled plasma optical emission spectrometry on an Agilent 5800 VDV ICP-OES (Agilent, Santa Clara, CA, USA) system after acid digestion with H_2SO_4 and HF (both from Scharlau, Barcelona, Spain). Textural properties were evaluated by nitrogen physisorption at 77 K using a Micromeritics TRISTAR 3000 analyzer (Micromeritics, Norcross, GA, USA). The specific surface area was estimated by the BET method, and the total pore volume was determined at $P/P_0 = 0.95$. The pore size was estimated from the maximum BJH pore size distribution. To obtain information about the reducibility of the cobalt species, a temperature-programmed reduction (TPR) experiment was performed on a Micromeritics Autochem 2930 analyzer, heating at 10 °C/min up to 900 °C while flowing a 10% H_2/Ar mixture.

Hydrogen production from green methanol via oxidative reforming was carried out in a fixed-bed reactor (Microactivity PRO unit, PID Eng&Tech. S.L., Alcobendas, Madrid, Spain) using shaped catalyst pellets. The shaped catalyst consisted of seven cylindrical extrudates, approximately 25 mm in length and 3 mm in diameter, arranged axially inside a stainless-steel tubular reactor (ID: 9.2 mm, length: 300 mm). This ordered arrangement was intentionally adopted to improve the reproducibility of the catalytic tests by minimizing channeling effects and reducing hydrodynamic variability compared with conventional randomly packed beds, thereby facilitating catalyst performance evaluation under controlled operating conditions. To evaluate the influence of different operating variables, a design of experiments was implemented to assess the effects of the oxygen-to-carbon ratio (O_2/C), steam-to-carbon ratio (S/C), weight hourly space velocity (WHSV), and reaction temperature (T) on methanol conversion and hydrogen yield. This experimental design enables a systematic and efficient analysis of the individual and combined impact of these parameters, allowing the identification of the most significant factors and their interactions in the overall process performance. Each run of the experimental design corresponded to a unique combination of operating variables. Once steady-state operation was achieved, the response variables were determined from multiple analytical measurements and subsequently used for statistical analysis and model development. Before the reaction, the catalyst was activated under pure hydrogen up to 600 °C using a heating rate of 10 °C/min. Afterwards, nitrogen was flowed through the reactor until the desired reaction temperature (400, 500, or 600 °C) was reached. Then, a methanol–water mixture (S/C ratio of 1 or 2) was fed into the reactor at a WHSV of 30 or 45 h^{-1}—calculated from the total feed flow rate and the mass of active catalyst (excluding bentonite)—with nitrogen serving as both the carrier gas and the internal standard. The gas-phase composition was analyzed online using an Agilent 490 Micro-GC equipped with a PoraPlot U column (10 m), a molecular sieve 5A column (20 m), and a thermal conductivity detector (TCD). The condensed liquid fraction was collected downstream in a condenser and analyzed using an Agilent 7820A GC-FID equipped with a CP-WAX 52 CB column. The catalytic activity was evaluated through methanol conversion (Equation (4)) and H_2 yield (Equation (5)), which were used as the response variables for the DOE analysis and process evaluation. F_i represents the inlet or outlet molar flow rate of methanol or hydrogen.

$$X_{MetOH}(\%) = \frac{F_{MetOH,in} - F_{MetOH,out}}{F_{MetOH,in}} \cdot 100 \quad (4)$$

$$H_2 \text{ yield } (\%) = \frac{F_{H_2,out}}{3 \cdot F_{MetOH,in}} \cdot 100 \quad (5)$$

Finally, the amount of carbon deposited on the catalyst was determined gravimetrically. The coke formation rate was calculated from the amount of carbon removed, the catalyst mass, and the time-on-stream.

3. Results

3.1. Characterization of Co-Cr/SBA-15 Catalysts

Samples were denoted as Co-Cr/SBA-15 (x), where x corresponds to p for the powdered catalyst and s for the shaped sample. Table 1 summarizes the elemental composition determined by ICP-OES together with the textural properties of the catalysts. Regarding the metal content, the powdered sample shows 6.5 wt% Co and 1.7 wt% Cr, values very close to the nominal loadings used during synthesis. In contrast, for the Co-Cr/SBA-15 (s) catalyst, these values decrease markedly due to the dilution effect introduced by the 30% bentonite used as the inorganic binder. Nonetheless, when considering only the catalyst fraction within the pellet, the corresponding metal loadings are comparable to those of the powdered material. Additionally, the shaped material exhibited flexural strengths ranging from 1.9 to 2.5 MPa, indicating good mechanical integrity and adequate structural robustness despite its highly porous nature, thereby supporting its suitability for catalytic applications [30].

Table 1. Physicochemical properties of Co-Cr/SBA-15 (p) and Co-Cr/SBA-15 (s) catalysts.

Sample	% Co [a] (wt.%)	% Cr [a] (wt.%)	S_{BET} (m^2/g)	Vp [b] (cm^3/g)	Dp [c] (nm)	σ_{max} (MPa)
Co-Cr/SBA-15 (p)	6.5	1.7	460	0.76	7.4	-
Co-Cr/SBA-15 (s)	4.6	1.0	343	0.51	7.2	1.9–2.5 [d]

[a] Determined by ICP-OES; [b] determined at P/P_0 = 0.95; [c] determined from the maximum BJH distribution; [d] determined from four-point and three-point bending tests, respectively.

Figure 2A shows the nitrogen adsorption–desorption isotherms. The powder catalyst (Co-Cr/SBA-15 (p)) displays the characteristic profile of a type IV isotherm with an H1-type hysteresis loop, typical of materials with a well-ordered mesoporous structure such as SBA-15 used as support. The shaped sample (Co-Cr/SBA-15 (s)) also exhibits a type IV isotherm with an H1 hysteresis loop, indicating that the mesostructure of the powdered catalyst is preserved after the shaping process. The textural properties reported in Table 1 show a decrease in BET surface area for the shaped material. This reduction is mainly attributed to the partial dilution of the mesoporous structure of the powdered sample with the bentonite binder, whose laminar structure results in a significantly lower specific surface compared to the powdered catalyst [29]. In addition, the shaping process may cause partial pore blockage as previously reported [31,32], which also accounts for the observed decrease in pore volume for Co-Cr/SBA-15 (s). In contrast, the pore diameter determined from the maximum BJH distribution remains similar for both samples, further indicating that the SBA-15 mesoporous framework is preserved after both the active-phase impregnation and the extrusion process.

The reducibility of the catalysts was assessed by H_2-TPR, and the corresponding profiles are shown in Figure 2B. Both materials exhibit two clearly differentiated reduction regions: a low-temperature zone below approximately 400 °C and a second one at higher temperatures. In the low-temperature range, the main reduction peak appears between 318 and 337 °C and is attributed to the reduction of Co_3O_4 to CoO. At higher temperatures, a broad feature within the range 460–620 °C is associated with the subsequent reduction of CoO to metallic cobalt whose reduction can be slightly influenced by the presence of

chromium species [33]. The powdered catalyst (Co-Cr/SBA-15 (p)) also shows a small feature at 229 °C, assigned to the reduction of Cr-oxide species [33,34] whose reducibility can be influenced by the presence of Co_3O_4. This signal, however, is not observed in the extruded material. This can be explained by the higher calcination temperature used for the shaped materials, which commonly decreases the reducibility by modifying their crystallinity or promoting stronger interactions [35]. With regard to the main reduction events, the extruded catalyst shows a slight shift in the low-temperature peak toward higher values, consistent with the hindered reducibility of Co_3O_4 after the more severe thermal treatment used. Conversely, the high-temperature reduction peak shifts to somewhat lower temperatures, suggesting a weaker metal–support interaction [36]. Overall, the extrusion process preserves the fundamental reduction pattern of Co-Cr/SBA-15 (p), indicating that the redox properties of the cobalt–chromium species remain almost unaltered after shaping.

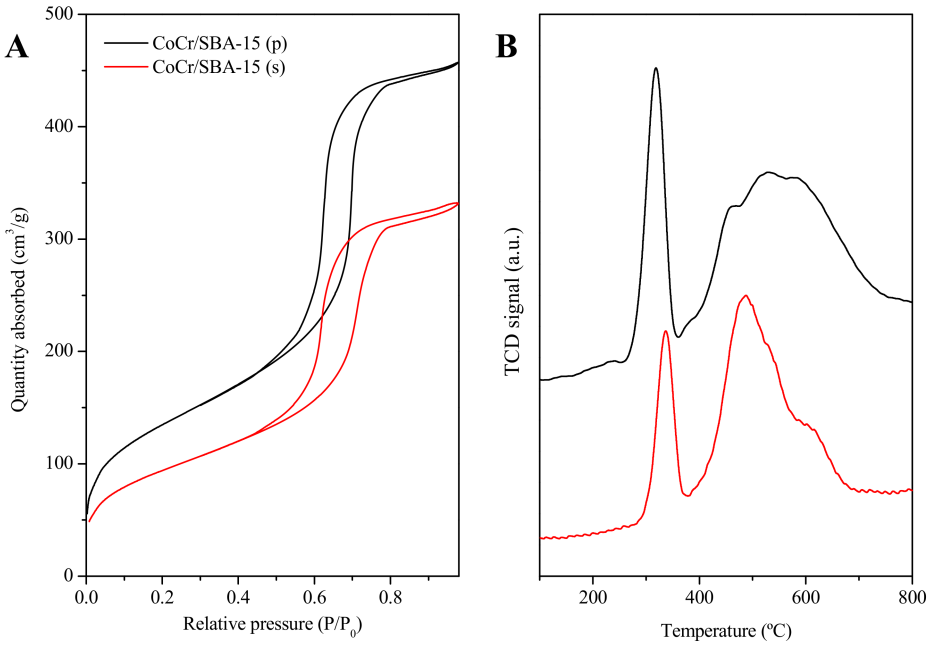


Figure 2. N_2 adsorption–desorption isotherms (**A**) and H_2-TPR profiles (**B**) of calcined Co-Cr/SBA-15 (p) and Co-Cr/SBA-15 (s) catalysts.

3.2. Catalytic Performance of Co-Cr/SBA-15 (s) in the Oxidative Steam Reforming of Methanol

For the oxidative reforming of methanol, all catalytic tests were performed using shaped catalysts, as their mechanical strength makes them more suitable for large-scale operations than powdered materials. Accordingly, a series of experiments was conducted to evaluate the influence of key operating variables—temperature, WHSV, S/C ratio, and O_2/C ratio—on catalytic performance, evaluated through methanol conversion and hydrogen yield. Based on experimental data acquired by varying operating conditions—O_2/C (0.10 and 0.15), WHSV (30 and 45 h^{-1}), S/C (1 and 2), and temperature (400, 500, and 600 °C)—response-surface plots were generated in Origin using the Convert to Matrix (XYZ Gridding) tool. These surfaces represent the experimental trends observed across the design space for each parameter combination, without applying any additional model fitting. In this regard, Figure 3 shows the experimental response surface for methanol conversion.

The results clearly show that increasing the O_2/C ratio leads to higher methanol conversion across all evaluated S/C ratios and temperatures, as evidenced by the higher values toward the lower-right of each contour surface plot. In oxidative steam reforming reactions, a higher O_2 content not only supplies heat—owing to the exothermic nature of

partial-oxidation reactions—but also promotes the oxidation pathways of methanol and its intermediates, thereby enhancing overall conversion. With respect to WHSV, lower values resulted in higher conversions because when the WHSV is low, the contact time is longer, which facilitates the reforming reaction towards products. Likewise, increasing temperature produces a pronounced rise in conversion, reaching near-complete conversion at 600 °C; this outcome is consistent with the endothermic nature of the methanol steam reforming reaction, making it thermodynamically favored at higher temperatures. Finally, comparing the results at S/C = 1 with those at S/C = 2 provides evidence that a higher S/C improves methanol conversion, as additional steam shifts the equilibrium toward products in accordance with Le Chatelier's principle [37].

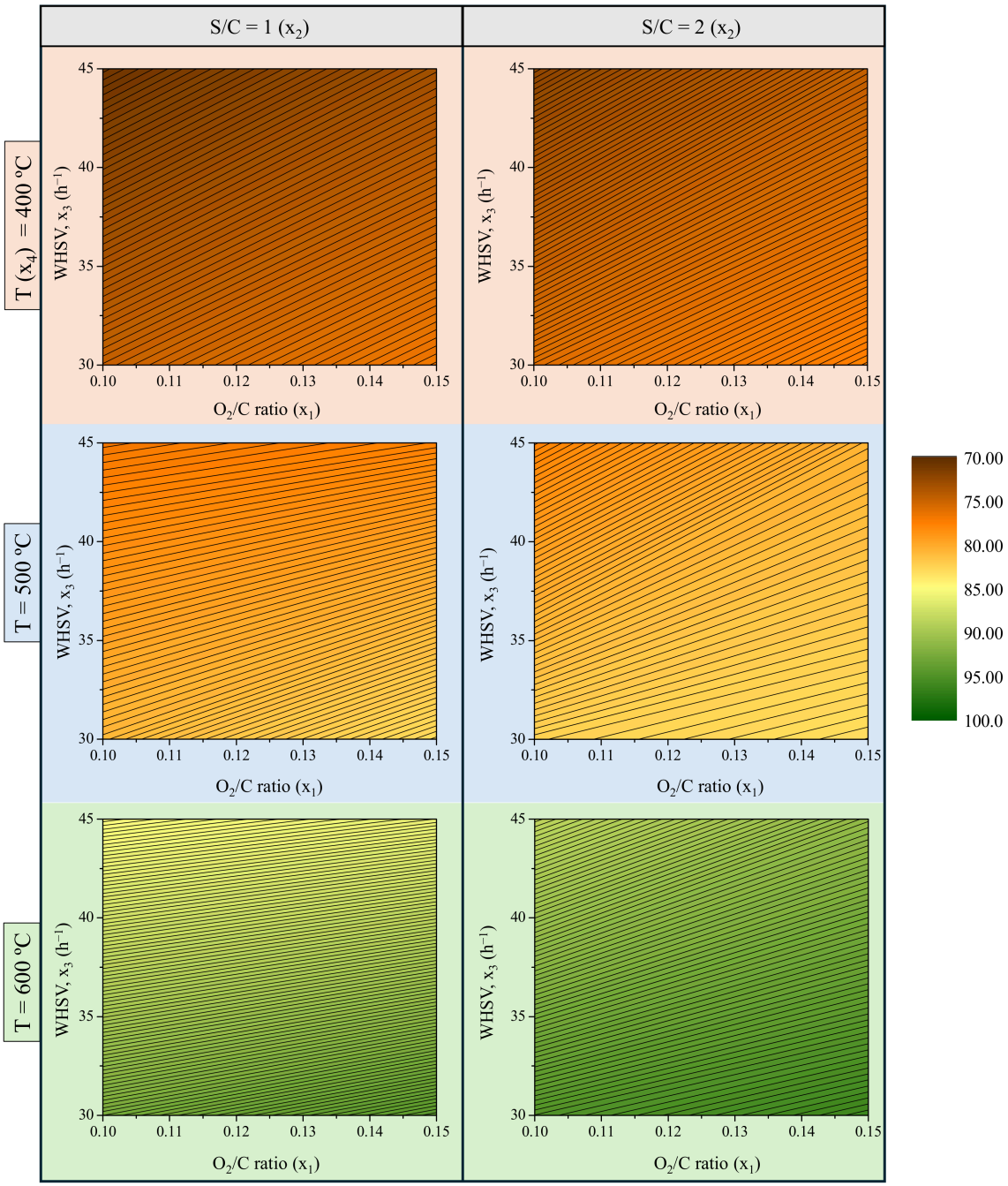


Figure 3. Contour response-surface plots of methanol conversion (%) vs. O_2/C and WHSV at S/C = 1–2 and T = 400–600 °C using Co-Cr/SBA-15 (s). Columns correspond to S/C ratios of 1 and 2, while rows correspond to temperatures of 400, 500, and 600 °C.

With respect to hydrogen yield, experimental contour response-surface plots as a function of the operating conditions are shown in Figure 4. Consistent with the behavior observed for conversion, increasing temperature, decreasing the WHSV, and increasing the S/C ratio led to higher hydrogen yields, with temperature showing the strongest influence. This is evident from the pronounced variations observed when comparing response surfaces at fixed S/C at different temperatures.

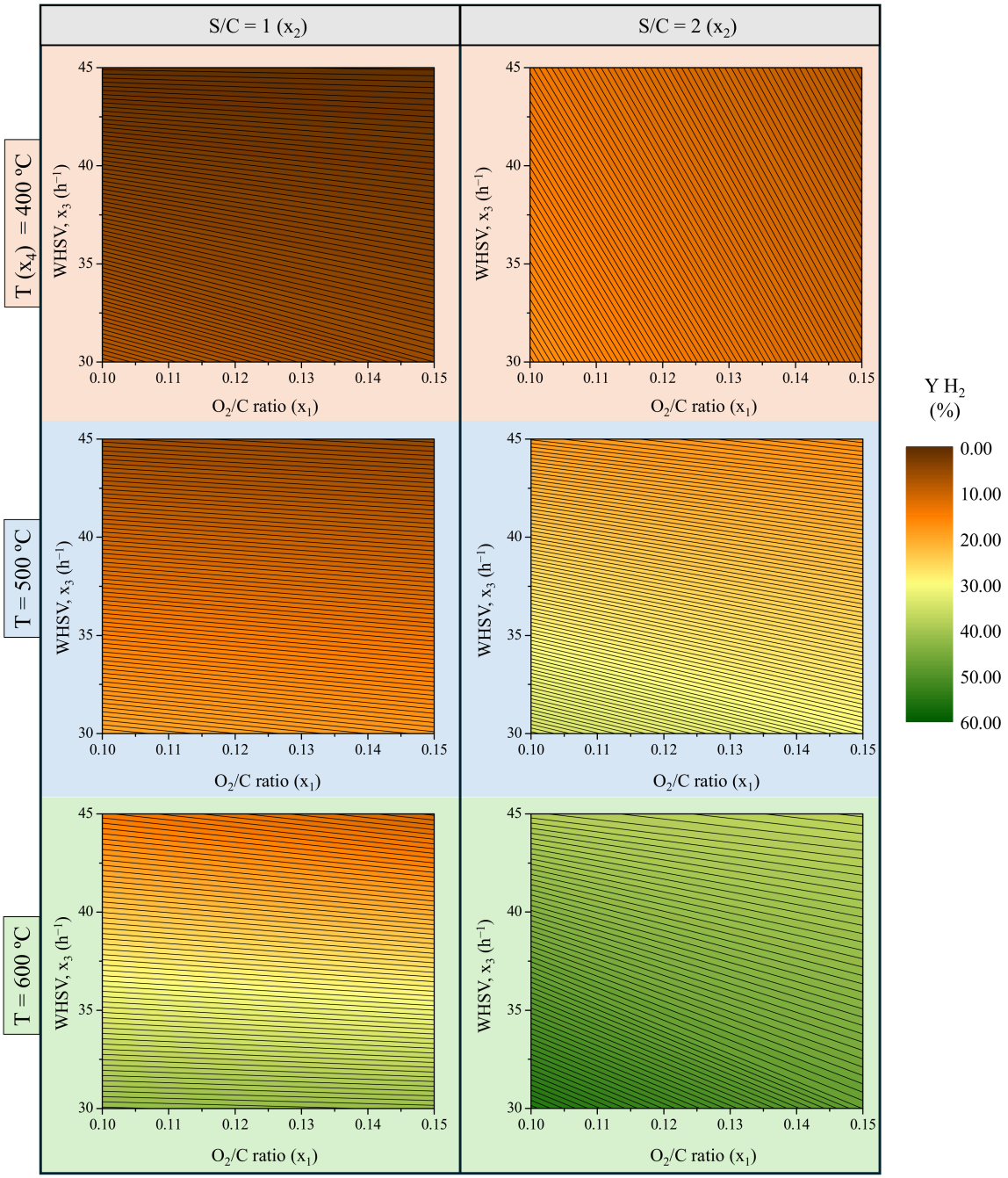


Figure 4. Contour response-surface plots of H_2 yield (%) vs. O_2/C and WHSV at S/C = 1–2 and T = 400–600 °C using Co-Cr/SBA-15 (s). Columns correspond to S/C ratios of 1 and 2, while rows correspond to temperatures of 400, 500, and 600 °C.

Regarding space velocity, lower WHSV favors hydrogen production, especially at elevated temperatures, consistent with the endothermic nature of steam reforming. However, in contrast to conversion, increasing O_2/C has a detrimental effect on hydrogen yield,

which is expected because oxygen oxidizes not only methanol—thus increasing methanol conversion—but also the hydrogen produced through methanol steam reforming and water–gas shift reactions.

3.3. Design of Experiments

To better understand the catalytic results described above, it is useful to analyze how the different operational variables influence the system. For this purpose, a design-of-experiments approach was applied, allowing the systematic evaluation of the factors affecting catalyst performance. In this respect, Table 2 summarizes the 24-run factorial design ($2 \times 2 \times 2 \times 3$) combining three two-level factors—O_2/C (0.10, 0.15), S/C (1, 2), and WHSV (30, 45 h^{-1})—with a three-level temperature factor (400, 500, 600 °C).

Table 2. Experimental design matrix (mixed factorial $2^3 \times 3$): runs, real factor levels, and coded variables (x_1–x_4).

Run	O_2/C	S/C	WHSV (h^{-1})	T (°C)	x_1 (O_2/C)	x_2 (S/C)	x_3 (WHSV)	x_4 (T)
1	0.10	1	45	400	−1	−1	1	−1
2	0.15	1	45	400	1	−1	1	−1
3	0.10	1	30	400	−1	−1	−1	−1
4	0.15	1	30	400	1	−1	−1	−1
5	0.10	2	45	400	−1	1	1	−1
6	0.15	2	45	400	1	1	1	−1
7	0.10	2	30	400	−1	1	−1	−1
8	0.15	2	30	400	1	1	−1	−1
9	0.10	1	45	500	−1	−1	1	0
10	0.15	1	45	500	1	−1	1	0
11	0.10	1	30	500	−1	−1	−1	0
12	0.15	1	30	500	1	−1	−1	0
13	0.10	2	45	500	−1	1	1	0
14	0.15	2	45	500	1	1	1	0
15	0.10	2	30	500	−1	1	−1	0
16	0.15	2	30	500	1	1	−1	0
17	0.10	1	45	600	−1	−1	1	1
18	0.15	1	45	600	1	−1	1	1
19	0.10	1	30	600	−1	−1	−1	1
20	0.15	1	30	600	1	−1	−1	1
21	0.10	2	45	600	−1	1	1	1
22	0.15	2	45	600	1	1	1	1
23	0.10	2	30	600	−1	1	−1	1
24	0.15	2	30	600	1	1	−1	1

Catalyst geometry was kept constant during all experiments and, therefore, was not included as a factor in the design of experiments. This factorial design was used to evaluate the relationship between the operating conditions and the resulting methanol conversion and hydrogen yield. For analysis, variables were coded as x_1 (O_2/C), x_2 (S/C), x_3 (WHSV)

and x_4 (T); the two-level factors use −1 (low) and +1 (high), and temperature is centered at 500 °C and scaled so that −1, 0, and +1 correspond to 400, 500, and 600 °C, respectively. Presenting the operating (absolute) settings alongside their coded counterparts links the statistical model to the practical operating space, makes effect estimates comparable across factors, and aids reproducibility.

Based on the experimental results, linear terms were fitted for x_1, x_2 and x_3, while a quadratic term was used for x_4 because the three levels allow the estimation of curvature. Accordingly, conversion and hydrogen yield were modeled as polynomial functions of the coded factors, enabling direct interpretation of each variable's influence on the process as given by Equation (6).

$$y = \beta_0 + \beta_1 \cdot x_1 + \beta_2 \cdot x_2 + \beta_3 \cdot x_3 + \beta_4 \cdot x_4 + \beta_{12} \cdot x_1 \cdot x_2 + \beta_{13} \cdot x_1 \cdot x_3 + \beta_{14} \cdot x_1 \cdot x_4 + \beta_{23} \cdot x_2 \cdot x_3 + \beta_{24} \cdot x_2 \cdot x_4 + \beta_{34} \cdot x_3 \cdot x_4 + \beta_{44} \cdot {x_4}^2 \quad (6)$$

Using least-squares regression, all β parameters were estimated according to Equations (7) and (8). The intercept β_0 is referenced to the center point x_0; accordingly, its value equals the mean conversion or hydrogen yield at 500 °C. By contrast, the quadratic temperature coefficient β_{44}, associated with ${x_4}^2$, was estimated as the difference between the average response at the extreme temperatures (400 and 600 °C) with the center-point mean (500 °C) as shown in Equation (9).

$$\beta_i = \frac{\bar{y}(x_i = +1) - \bar{y}(x_i = -1)}{2} \quad (7)$$

$$\beta_{ij} = \frac{\bar{y}(x_i \cdot x_j = +1) - \bar{y}(x_i x_j = -1)}{2} \quad (8)$$

$$\beta_{44} = \frac{\bar{y}_{400} + \bar{y}_{600}}{2} - \bar{y}_{500} \quad (9)$$

By applying this procedure to the two response variables—methanol conversion and hydrogen yield—the corresponding intercepts were estimated, leading to Equations (10) and (11), which define the models for methanol conversion (X_{MetOH}) and hydrogen yield (Y_{H2}), respectively.

$$X_{MetOH} = 80.2450 + 0.8833 \cdot x_1 + 0.9475 \cdot x_2 - 2.4383 \cdot x_3 + 8.2850 \cdot x_4 + 0.0542 \cdot x_1 \cdot x_2 + 0.0900 \cdot x_1 \cdot x_3 - 0.1000 \cdot x_1 \cdot x_4 + 0.3392 \cdot x_2 \cdot x_3 + 0.5037 \cdot x_2 \cdot x_4 - 0.8225 \cdot x_3 \cdot x_4 + 2.5475 \cdot {x_4}^2 \quad (10)$$

$$Y_{H2} = 18.5363 - 1.4950 \cdot x_1 + 6.4750 \cdot x_2 - 6.7142 \cdot x_3 + 13.8156 \cdot x_4 - 0.7283 \cdot x_1 \cdot x_2 + 0.4008 \cdot x_1 \cdot x_3 - 0.1000 \cdot x_1 \cdot x_4 + 0.3392 \cdot x_2 \cdot x_3 + 0.5037 \cdot x_2 \cdot x_4 - 0.8225 \cdot x_3 \cdot x_4 + 2.5475 \cdot {x_4}^2 \quad (11)$$

To determine which operating variables most strongly influence performance and identify relevant interactions or curvature effects, a hierarchical second-order linear model was applied and a Type-II ANOVA was performed for each response variable (see Table 3). This ANOVA divides the explainable variation into main effects, two-factor interactions, and the quadratic temperature term, which is the only squared term that can be estimated with the three temperature levels used. The residual mean square of the full model was used as the reference error. Since no independent replicate experiments were included in the design, the residual error term represents the unexplained variation after model fitting and may therefore include contributions from both experimental variability and model inadequacy. Consequently, pure experimental error and lack-of-fit cannot be independently estimated within the present experimental design. It is important to highlight that *p*-values

< 0.05 denote significant model terms; moreover, higher F values coupled with smaller *p*-values indicate a stronger contribution to the quadratic model.

Table 3. Model ANOVA II for conversion and H_2 yield: sums of squares, F-statistics, *p*-values, and significance.

Conversion				
Source	**Sum of Squares**	**F**	***p***	**Significance**
x_1	18.727	36.285	6.00×10^{-5}	***
x_2	21.546	41.748	3.11×10^{-5}	***
x_3	142.691	276.477	1.19×10^{-9}	***
x_4	1098.260	2127.978	7.031×10^{-15}	***
$x_1 \cdot x_2$	0.070	0.136	0.718	-
$x_1 \cdot x_3$	0.194	0.377	0.551	-
$x_1 \cdot x_4$	0.160	0.310	0.588	-
$x_2 \cdot x_3$	2.761	5.349	0.039	*
$x_2 \cdot x_4$	4.060	7.867	0.016	*
$x_3 \cdot x_4$	10.824	20.973	6.33×10^{-4}	***
x_4^2	34.612	67.064	2.96×10^{-6}	***
Residual	6.193	-	-	-
Hydrogen Yield				
Source	**Sum of Squares**	**F**	***p***	**Significance**
x_1	53.641	6.733	0.023	*
x_2	1006.215	126.307	1.000×10^{-7}	***
x_3	1081.921	135.810	6.697×10^{-8}	***
x_4	3053.944	383.352	1.787×10^{-10}	***
$x_1 \cdot x_2$	12.731	1.598	0.230	-
$x_1 \cdot x_3$	3.856	0.484	0.500	-
$x_1 \cdot x_4$	0.013	0.002	0.969	-
$x_2 \cdot x_3$	50.402	6.327	0.027	*
$x_2 \cdot x_4$	77.220	9.693	0.009	**
$x_3 \cdot x_4$	296.442	37.211	5.335×10^{-5}	***
x_4^2	60.055	7.538	0.018	*
Residual	95.597	-	-	-

* p <0.05; ** p < 0.01; *** p < 0.001.

The results show that temperature (x_4) is the dominant factor for both responses. The effect of temperature is highly significant for both methanol conversion and hydrogen yield, as evidenced by the clear positive curvature associated with the positive coefficient of x_4^2 in Equation (5). This indicates that the improvement from 500 °C to 600 °C is larger than from 400 °C to 500 °C. WHSV (x_3) also shows a clear main effect with a negative sign in both models, meaning that lower WHSV values improve conversion and hydrogen yield within the studied range. The influence of S/C (x_2) is present in both responses, but it is particularly important for the hydrogen yield, as higher steam concentrations shift the reaction toward products. Differences between the two responses arise when evaluating

O_2/C (x_1). For conversion, it is significant and has a positive coefficient, indicating that increasing the O_2/C ratio enhances conversion. In contrast, for hydrogen yield, although it is significant, it has a negative coefficient, implying that higher O_2/C ratios adversely affect the hydrogen produced. However, consideration of the individual effects alone is insufficient because significant interactions exist between several variables, particularly between WHSV and temperature ($x_3 \cdot x_4$), between S/C and temperature ($x_2 \cdot x_4$), and, to a lesser extent, between S/C ratio and WHSV ($x_2 \cdot x_3$). These interactions show that the process reaches its highest methanol conversion and hydrogen production when the system operates at high temperature, low WHSV, and high S/C, while keeping O_2/C lower to avoid excessive oxidation of the produced hydrogen. These interaction effects can also be interpreted from a process perspective. The significance of the WHSV and temperature interaction ($x_3 \cdot x_4$) reflects the combined influence of reaction kinetics and residence time. At higher temperatures, reaction rates increase substantially, partially compensating for the shorter contact times associated with elevated WHSV values. Conversely, at lower temperatures, the reduction in residence time has a more pronounced negative impact on methanol conversion and hydrogen production. The significance of the S/C and temperature interaction ($x_2 \cdot x_4$) suggests that the influence of steam depends on the thermal conditions within the reactor. At higher temperatures, additional steam more effectively promotes steam reforming reactions and hydrogen production due to the faster reaction kinetics. In contrast, at lower temperatures, the influence of steam becomes less pronounced because the reaction rates are intrinsically slower. Similarly, the S/C and WHSV interaction ($x_2 \cdot x_3$) highlights the combined importance of steam availability and contact time. The beneficial effect of increasing the S/C ratio is more pronounced at lower WHSV values, where longer residence times allow the reforming reactions to proceed to a greater extent.

To simplify, the model terms with $p < 0.05$ are retained, while those without evidence of effect are removed, always respecting hierarchy (if an interaction remains, its main effects are kept). Consequently, Equations (12) and (13) define the model for methanol conversion and hydrogen yield, respectively.

$$X_{MetOH} = 80.2450 + 0.8833 \cdot x_1 + 0.9475 \cdot x_2 - 2.4383 \cdot x_3 + 8.2850 \cdot x_4 + 0.3392 \cdot x_2 \cdot x_3 + 0.5037 \cdot x_2 \cdot x_4 - 0.8225 \cdot x_3 \cdot x_4 + 2.5475 \cdot {x_4}^2 \quad (12)$$

$$Y_{H2} = 18.5363 - 1.4950 \cdot x_1 + 6.4750 \cdot x_2 - 6.7142 \cdot x_3 + 13.8156 \cdot x_4 + 1.4492 \cdot x_2 \cdot x_3 + 2.1969 \cdot x_2 \cdot x_4 - 4.3044 \cdot x_3 \cdot x_4 + 3.3556 \cdot {x_4}^2 \quad (13)$$

The reduced models expressed in Equations (12) and (13) are formulated in terms of the coded variables x_1, x_2, x_3, and x_4. For practical application of these models, the operating variables must first be converted into their corresponding coded values according to Equation (14).

$$x_i = \frac{X_i - X_0}{\Delta} \quad (14)$$

where X_i refers to the operating condition under evaluation (O_2/C, S/C, WHSV or T); X_0 is the midpoint—i.e., the mean of the minimum and maximum levels in the design—and Δ is half the range, $\Delta = (X_{max} - X_{min})/2$.

Agreement between predictions and experimental data is evident in Figure 5 for both conversion (A) and hydrogen yield (B), where the data points closely follow the y = x parity line with only minor dispersion. This behavior is consistent with high predictive fidelity and indicates the absence of systematic error across the explored operating domain. Consistent with this observation, Table 4 summarizes the goodness-of-fit and predictive performance metrics for both responses. The high adjusted R^2 values, together with the

reasonably close predicted R^2, indicate that the models explain most of the observed variability while maintaining good predictive capability within the experimental domain. Furthermore, the close agreement between predicted and experimental values supports the adequacy of the fitted models for describing the behavior of the system under the operating conditions considered. Therefore, the developed models are suitable for interpretation and prediction within the experimental region explored in this study, whereas extrapolation beyond these ranges should be approached with caution. Specifically, the proposed models should only be applied within the investigated ranges of the O_2/C ratio (0.10–0.15), S/C ratio (1–2), WHSV (30–45 h^{-1}), and temperature (400–600 °C), as their applicability beyond this experimental domain has not been verified. Another parameter used to assess model adequacy is Adequate Precision, which quantifies the signal-to-noise ratio of the model predictions and should exceed a value of 4 for an accurate model [38], meaning that the spread of the model's predictions is at least four times larger than the typical prediction error, ensuring that the model can resolve effects and guide optimization reliably. In this study, both responses exceeded this threshold by a wide margin—47.81 for methanol conversion and 34.15 for hydrogen yield—further supporting the predictive capability of the developed models within the investigated experimental region.

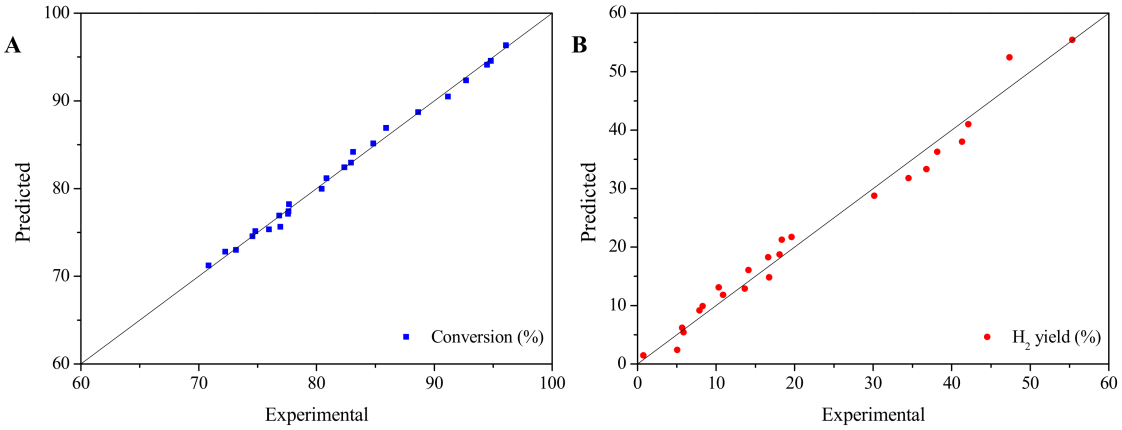


Figure 5. Parity plots (predicted vs. experimental) for (**A**) conversion (%) and (**B**) H_2 yield (%). The diagonal line denotes the identity y = x.

Table 4. Model fit and validation metrics for methanol conversion and H_2 yield.

	Methanol Conversion	**H_2 Yield**
R^2	0.995	0.981
Adjusted R^2	0.991	0.970
Predicted R^2	0.995	0.948
Adequate Precision	47.81	34.15

To further support the accuracy of the model, the study examines standardized residuals. These residuals are obtained by scaling each raw residual by the estimated standard deviation and the leverage of the corresponding observation, placing all residuals on a common scale. This transformation facilitates the identification of unusual points and enables the evaluation of key statistical assumptions—such as normality and constant variance—that cannot be confirmed by the R^2 value alone. In practice, a rough symmetric distribution around zero and the absence of large values—i.e., response outliers ($|r_i| \geq 3$) [39,40]—suggest that the model is capturing the main structure of the data. Conversely, any systematic trend or structure in the residuals would indicate that the model still

does not fit the data properly. Thus, standardized residuals provide a clearer, more reliable check that the final specification is both statistically sound and predictively robust within the experimental range evaluated. To visually examine these assumptions, Q-Q plots of the standardized residuals were constructed by comparison with the theoretical quantiles of a normal distribution. If the residuals follow an approximately normal distribution—an assumption required for the F-tests and confidence intervals—the data points should align closely with the 45° reference line, with only minor deviations due to sampling variability. Figure 6A,B show the corresponding Q-Q plots for methanol conversion and hydrogen yield, respectively.

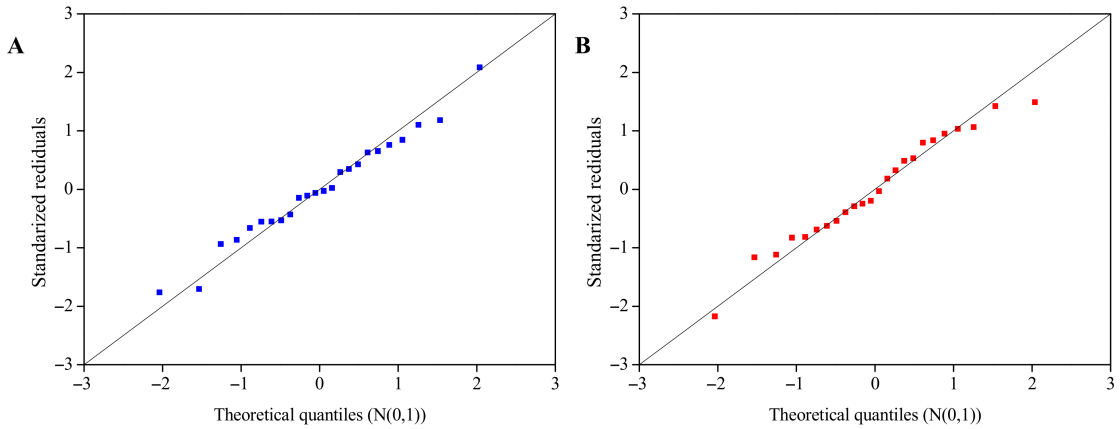


Figure 6. Q-Q plots of standardized residuals versus theoretical quantiles of N(0,1): (**A**) methanol conversion and (**B**) H_2 yield. The diagonal line denotes the identity y = x.

In both cases, the QQ plot displays an almost linear pattern with small and symmetric deviations at the extremes—as expected for a sample size of n = 24—and no signs of systematic curvature or "S-shape" behavior. Combined with the absence of large residual outliers ($|r_i| \geq 3$) and the strong predictive indicators obtained (high predicted R^2 and an Adequate Precision value above the typical threshold), these results confirm that the final reduced models successfully capture the systematic behavior of the experimental data and provide reliable predictions within the investigated design space. Additional diagnostic plots of standardized residuals versus experimental run order and predicted values are presented in Figures S1 and S2, respectively. The residuals were randomly distributed around zero, with no discernible trends, substantial heteroscedasticity, or dependence associated with the experimental sequence, further supporting the validity of the model assumptions.

In summary, the fitted models were used to evaluate all 24 combinations within the range of conditions tested and identify the operating conditions that maximize each response. For methanol conversion, the best performance takes place at O_2/C = 0.15, S/C = 2, WHSV = 30 h^{-1}, and 600 °C, yielding a predicted conversion of 96.33%, consistent with the closest experimental value of 96.09%. For hydrogen yield, the optimal point shifts slightly to a lower O_2/C ratio of 0.10 while maintaining S/C = 2, WHSV = 30 h^{-1}, and 600 °C, resulting in a predicted yield of 55.44% (near the observed 55.37%) and a predicted conversion of 94.57%. When looking for a balanced solution between both responses, an O_2/C = 0.15, S/C = 2, WHSV = 30 h^{-1}, and T = 600 °C as experimental conditions provide a good compromise, achieving 96.33% conversion and 52.45% hydrogen yield. The latter corresponds to a desirability value of 0.95, indicating that the selected operating conditions achieve approximately 95% of the maximum attainable hydrogen yield within the investigated experimental domain, while simultaneously maintaining 100% of the maximum predicted methanol conversion. Overall, the DOE analysis indicates

that maximizing hydrogen yield without severely compromising conversion is favored by high temperature, low WHSV, S/C = 2, and a relatively low O_2/C ratio of approximately 0.10. In contrast, when the primary objective is maximum conversion, increasing O_2/C to 0.15 is preferred.

Based on the DOE results, the operating conditions that maximize hydrogen yield were selected as a reference point to verify the consistency of catalytic performance across different catalyst forms. Under these optimal conditions (O_2/C = 0.10, S/C = 2, WHSV = 30 h^{-1}, and T = 600 °C), the performance of the agglomerated catalyst was compared with that of the corresponding powdered material, and the experimental results were contrasted with the values predicted by the DOE model. In this respect, Figure 7 presents the methanol conversion and hydrogen yield obtained over Co-Cr/SBA-15 (p) and Co-Cr/SBA-15 (s), together with the corresponding model predictions for the shaped material.

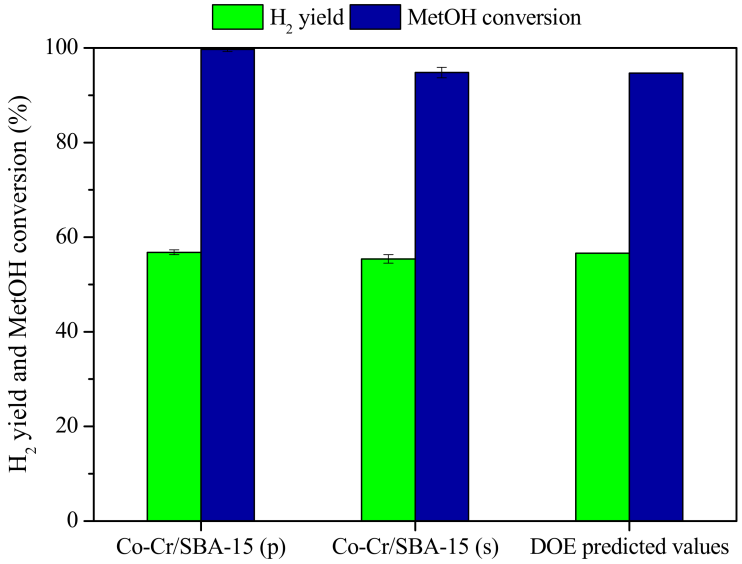


Figure 7. Methanol conversion and hydrogen yield obtained over agglomerated and powdered Co-Cr/SBA-15 catalysts under the optimum operating conditions for hydrogen production, together with the values predicted by the DOE model. Error bars represent analytical variability associated with the measurements.

Good agreement between the experimental and predicted values was observed, providing experimental verification of the model predictions under the selected operating conditions and further supporting the suitability of the DOE model within the investigated operating domain. The comparison between the powdered and shaped catalysts was performed under identical operating conditions and using equivalent amounts of active catalyst. While the powdered catalyst exhibited slightly higher methanol conversion than the agglomerated material, the difference was relatively small and did not result in an appreciable variation in hydrogen yield, which remained essentially unchanged for both catalyst forms. Despite the lower BET surface area and pore volume resulting from the incorporation of bentonite during catalyst shaping, the shaped catalyst maintained hydrogen yields close to those obtained with the powdered catalyst under the selected operating conditions, indicating that catalyst shaping preserved high catalytic performance. These findings indicate that the overall catalytic performance was largely preserved after shaping, despite the textural modifications associated with bentonite incorporation. However, although the shaped catalyst performed effectively under the optimal operating conditions identified by the DOE model, its suitability for industrial application must also be assessed through long-term stability studies. In practical applications, catalysts are required to operate continuously for extended periods while maintaining their activity and

selectivity. Therefore, a 50 h time-on-stream experiment was carried out under the optimum hydrogen-production conditions to assess the stability of the Co-Cr/SBA-15 (s) catalyst under the investigated reaction conditions. As shown in Figure 8, methanol conversion remained relatively stable throughout the 50 h time-on-stream experiment, decreasing by only about 5% relative to its initial value. In contrast, the hydrogen yield remained nearly constant over the entire test, indicating that hydrogen production was essentially unaffected. These results demonstrate the stability of the Co-Cr/SBA-15 (s) catalyst over 50 h time-on-stream under the optimized reaction conditions.

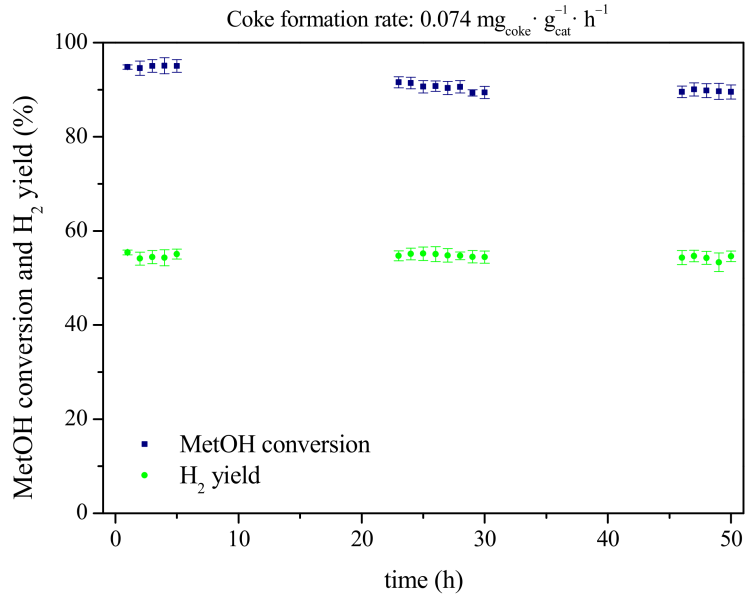


Figure 8. Stability test of Co-Cr/SBA-15 (s) catalyst. Time-on-stream evolution of methanol conversion and hydrogen yield at atmospheric pressure, 600 °C, S/C = 2, O_2/C = 0.1, and WHSV = 30 h^{-1}. Error bars represent analytical variability associated with the measurements.

The stability results can be further understood by considering the extent of carbon deposition during operation. Figure 9 also reports a coke formation rate of only 0.074 $mg_{coke} \cdot g_{cat}{}^{-1} \cdot h^{-1}$, evidencing a negligible degree of carbon accumulation under the studied conditions. Such a limited amount of carbon deposition suggests that coke deposition was unlikely to account for the slight decrease in methanol conversion observed during the stability test. To further investigate possible changes in the catalyst during operation, the crystalline structures of the fresh reduced and spent catalysts were examined by XRD. The corresponding diffractograms are presented in Figure 9. The XRD patterns reveal that the main diffraction peaks in both samples can be assigned to bentonite [41] and metallic cobalt (JCPDS 00-001-1259), indicating that the crystalline structure of the catalyst remained essentially unchanged. Furthermore, no diffraction peaks associated with graphitic carbon were detected in the spent catalyst, in agreement with the very low coke formation rate discussed above. Beyond the qualitative comparison of the diffraction patterns, the average cobalt crystallite size was estimated using the Scherrer equation applied to the Co^0 (111) diffraction peak at $2\theta = 44.2°$. The calculated crystallite sizes, reported in Figure 9, were 7.4 nm for the fresh reduced catalyst and 7.7 nm for the spent catalyst. The similarity between these values—corresponding to an increase of only about 4%—indicates that cobalt sintering was very limited. Together with the negligible coke formation rate, these results support the good stability of the Co-Cr/SBA-15 (s) catalyst under the investigated conditions, as evidenced by the limited decrease in methanol conversion and the nearly constant hydrogen yield throughout the 50 h time-on-stream experiment. Nevertheless, the slight decrease in methanol conversion observed during the stability test

suggests that additional deactivation phenomena may be involved beyond the limited coke deposition and cobalt sintering detected. Possible contributors include changes in catalyst accessibility, modifications associated with the bentonite binder, partial pore blockage or transport-related effects during operation. Although the present results do not allow the origin of the observed conversion loss to be established unequivocally, the contribution of these effects cannot be excluded.

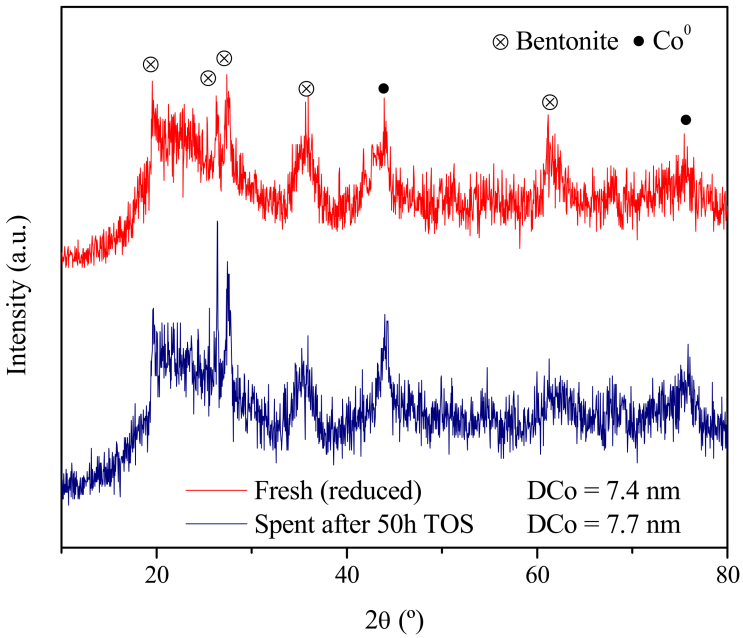


Figure 9. Comparison of the XRD patterns of the reduced and spent Co-Cr/SBA-15 (s) catalysts after the 50 h stability test.

4. Conclusions

Hydrogen production from green methanol via oxidative reforming was systematically investigated over agglomerated Co-Cr/SBA-15 catalysts by combining experimental evaluation with a factorial design-of-experiments methodology. The statistical analysis enabled the quantification of both the individual and interaction effects of the main operating variables—temperature, WHSV, S/C, and O_2/C—on methanol conversion and hydrogen yield. Among them, temperature was identified as the most influential factor, followed by WHSV, with higher temperatures and lower space velocities significantly enhancing catalytic performance. Increasing the S/C ratio promoted hydrogen production, whereas the O_2/C ratio exhibited a dual effect, improving methanol conversion while decreasing hydrogen yield due to the increased contribution of oxidation reactions. Consequently, the optimum conditions for hydrogen production were established at 600 °C, a WHSV of 30 h^{-1}, S/C = 2, and an O_2/C ratio of 0.10, while maximum methanol conversion was obtained at higher O_2/C values. The predictive capability of the reduced DOE models was assessed through parity plots, residual analysis, Adequate Precision, and experimental verification of the model predictions under the selected operating conditions. Under the optimum hydrogen-production conditions, the agglomerated catalyst exhibited catalytic performance comparable to that of its powdered counterpart, with experimental results in close agreement with model predictions. Overall, the proposed DOE approach proved to be an effective tool for optimizing and predicting the performance of Co-Cr/SBA-15 catalysts under fixed-bed operating conditions. The developed statistical models are applicable only within the investigated experimental domain and should not be extrapolated beyond the studied ranges of O_2/C ratio, S/C ratio, WHSV, and temperature without addi-

tional experimental validation. In addition, the shaped Co-Cr/SBA-15 catalyst exhibited stable performance over 50 h time-on-stream under the investigated reaction conditions, retaining approximately 95% of its initial methanol conversion while maintaining a nearly unchanged hydrogen yield. Furthermore, coke formation and cobalt sintering were negligible throughout the stability test, indicating only minor physicochemical modifications of the catalyst during operation. These results demonstrate that catalyst shaping with bentonite preserves the catalytic performance of Co-Cr/SBA-15 without compromising its stability, while highlighting the effectiveness of combining catalyst shaping and DOE-based optimization to identify favorable operating conditions for hydrogen production within the investigated experimental domain.

Supplementary Materials: The following supporting information can be downloaded at: https://www.mdpi.com/article/10.3390/cleantechnol8060175/s1. Figure S1. Standardized residuals vs run order of methanol conversion and H_2 yield; Figure S2. Standardized residuals vs predicted values of methanol conversion and H_2 yield.

Author Contributions: P.J.M.: Conceptualization, Methodology, Investigation, Formal Analysis, Data Curation, Writing—Original Draft Preparation, Writing—Reviewing and Editing. Á.M.d.l.C.: Investigation, Data Curation, Writing—Reviewing and Editing. A.J.V.: Data curation, Writing—Reviewing and Editing. J.A.C.: Funding Acquisition, Writing—Reviewing and Editing. A.C.: Visualization, Supervision, Data Curation, Conceptualization, Methodology, Writing—Reviewing and Editing, Funding Acquisition. All authors have read and agreed to the published version of the manuscript.

Funding: The authors acknowledge the financial support from the Ministry of Science, Innovation and Universities of Spain through the project PID2023-146597OB-I00.

Institutional Review Board Statement: Not applicable.

Informed Consent Statement: Not applicable.

Data Availability Statement: Open access data is available at https://doi.org/10.21950/TWMUB1.

Conflicts of Interest: The authors declare no conflicts of interest.

References

1. Megía, P.J.; Vizcaíno, A.J.; Calles, J.A.; Carrero, A. Hydrogen Production Technologies: From Fossil Fuels toward Renewable Sources. A Mini Review. *Energy Fuels* **2021**, *35*, 16403–16415. [CrossRef]
2. Cullen, D.A.; Neyerlin, K.C.; Ahluwalia, R.K.; Mukundan, R.; More, K.L.; Borup, R.L.; Weber, A.Z.; Myers, D.J.; Kusoglu, A. New Roads and Challenges for Fuel Cells in Heavy-Duty Transportation. *Nat. Energy* **2021**, *6*, 462–474. [CrossRef]
3. Sun, H.; Wang, Z.; Meng, Q.; White, S. Advancements in Hydrogen Storage Technologies: Enhancing Efficiency, Safety, and Economic Viability for Sustainable Energy Transition. *Int. J. Hydrogen Energy* **2025**, *105*, 10–22. [CrossRef]
4. Ur Rehman, M.A.; Schwarz, C.H.; Souzani, S.; Heßke, C.; Haumann, M. Methanol-to-Electricity via Low-Temperature Steam Reforming Integrated with a High-Temperature PEM Fuel Cell. *Sustain. Energy Fuels* **2025**, *9*, 5627–5634. [CrossRef]
5. Schorn, F.; Breuer, J.L.; Samsun, R.C.; Schnorbus, T.; Heuser, B.; Peters, R.; Stolten, D. Methanol as a Renewable Energy Carrier: An Assessment of Production and Transportation Costs for Selected Global Locations. *Adv. Appl. Energy* **2021**, *3*, 100050. [CrossRef]
6. Goeppert, A.; Czaun, M.; Jones, J.P.; Surya Prakash, G.K.; Olah, G.A. Recycling of Carbon Dioxide to Methanol and Derived Products—Closing the Loop. *Chem. Soc. Rev.* **2014**, *43*, 7995–8048. [CrossRef]
7. Adil, A.; Prasad, B.; Rao, L. Methanol Generation from Bio-Syngas: Experimental Analysis and Modeling Studies. *Environ. Dev. Sustain.* **2024**, *26*, 21503–21527. [CrossRef]
8. Yahyazadeh, A.; Nanda, S.; Dalai, A.K. A Critical Review of the Sustainable Production and Application of Methanol as a Biochemical and Bioenergy Carrier. *Reactions* **2024**, *5*, 1–19. [CrossRef]
9. Harkou, E.; Wang, H.; Manos, G.; Constantinou, A.; Tang, J. Advances in Catalyst and Reactor Design for Methanol Steam Reforming and PEMFC Applications. *Chem. Sci.* **2025**, *16*, 3810–3831. [CrossRef]
10. Farhan, S.M.; Wang, P.; Yin, J.J.; Chen, Z. Emerging Trends in Innovative Catalysts for Methanol Steam Reforming for Hydrogen Production: A Review of Recent Advances. *Energy* **2025**, *332*, 137042. [CrossRef]
11. Ma, X.; Yang, W.W.; Tang, X.Y.; He, Y.L. Solar-Driven Methanol Steam Reforming for Low Carbon and Efficient Hydrogen Production: A Review. *J. Clean. Prod.* **2024**, *436*, 140587. [CrossRef]

12. Deng, Y.; Li, S.; Appels, L.; Dewil, R.; Zhang, H.; Baeyens, J.; Mikulcic, H. Producing Hydrogen by Catalytic Steam Reforming of Methanol Using Non-Noble Metal Catalysts. *J. Environ. Manag.* **2022**, *321*, 116019. [CrossRef]
13. Megía, P.J.; Morales, A.; Vizcaíno, A.J.; Calles, J.A.; Carrero, A. Hydrogen Production through Oxidative Steam Reforming of Acetic Acid over Ni Catalysts Supported on Ceria-Based Materials. *Catalysts* **2022**, *12*, 1526. [CrossRef]
14. Megía, P.J.; Carrero, A.; Calles, J.A.; Vizcaíno, A.J. Hydrogen Production from Steam Reforming of Acetic Acid as a Model Compound of the Aqueous Fraction of Microalgae HTL Using Co-M/SBA-15 (M: Cu, Ag, Ce, Cr) Catalysts. *Catalysts* **2019**, *9*, 1013. [CrossRef]
15. Park, H.R.; Kim, B.J.; Ryu, S.J.; Jeon, Y.; Lee, S.S.; Bae, J.W.; Roh, H.S. Super-Dry Reforming of Methane over Surface Oxygen Mobility Enhanced Ni/MgO-Ce/SBA-15 Catalysts. *Catal. Today* **2025**, *453*, 115257. [CrossRef]
16. El Hassan, N.; Kaydouh, M.N.; Casale, S.; Banabdwin, K.M.; Alreshaidan, S.B.; Abahussain, A.A.M.; Al-Fatesh, A.S. Mesopore Confinement Does Not Stabilize Ni-Based Oxygen Carriers under High-Temperature Cyclic Redox Conditions: Amorphous SiO_2 versus Ordered SBA-15 in Chemical Looping Reforming of Methane. *Microporous Mesoporous Mater.* **2026**, *414*, 114339. [CrossRef]
17. Sohn, H.; Ozkan, U.S. Cobalt-Based Catalysts for Ethanol Steam Reforming: An Overview. *Energy Fuels* **2016**, *30*, 5309–5322. [CrossRef]
18. Megía, P.J.; Calles, J.A.; Carrero, A.; Vizcaíno, A.J. Effect of the Incorporation of Reducibility Promoters (Cu, Ce, Ag) in Co/CaSBA-15 Catalysts for Acetic Acid Steam Reforming. *Int. J. Energy Res.* **2021**, *45*, 1685–1702. [CrossRef]
19. Cortese, M.; Ruocco, C.; Palma, V.; Megía, P.J.; Carrero, A.; Calles, J.A. On the Support Effect and the Cr Promotion of Co Based Catalysts for the Acetic Acid Steam Reforming. *Catalysts* **2021**, *11*, 133. [CrossRef]
20. Carrero, A.; Vizcaíno, A.J.; Calles, J.A.; García-Moreno, L. Hydrogen Production through Glycerol Steam Reforming Using Co Catalysts Supported on SBA-15 Doped with Zr, Ce and La. *J. Energy Chem.* **2017**, *26*, 42–48. [CrossRef]
21. Reynoso, A.J.; Iriarte-Velasco, U.; Gutiérrez–Ortiz, M.A.; Ayastuy, J.L. Cobalt Aluminate Spinel-Derived Catalysts for Glycerol Steam Reforming. *J. Ind. Eng. Chem.* **2024**, *132*, 111–122. [CrossRef]
22. Chirinos, C.A.; Vizcaíno, A.J.; Calles, J.A.; Carrero, A.; Megía, P.J. Valorization of Bio-Oil Aqueous Fractions Through Oxidative Steam Reforming over Co/CeO2-SBA-15 Catalysts: From Single Model Compounds to Complex Mixtures. *Nanomaterials* **2026**, *16*, 85. [CrossRef]
23. Sayas, S.; Da Costa-Serra, J.F.; Chica, A. Sustainable Production of Hydrogen via Steam Reforming of Furfural (SRF) with Co-Catalyst Supported on Sepiolite. *Int. J. Hydrogen Energy* **2021**, *46*, 17481–17489. [CrossRef]
24. Calles, J.A.; Carrero, A.; Vizcaíno, A.J.; Megía, P.J. Agglomerated Co–Cr/SBA-15 Catalysts for Hydrogen Production through Acetic Acid Steam Reforming. *Int. J. Hydrogen Energy* **2020**, *45*, 15941–15950. [CrossRef]
25. Iro, E.; Hajimirzaee, S.; Sasaki, T.; Olea, M. Novel Ni/SBA-15 Catalyst Pellets for Tar Catalytic Cracking in a Dried Sewage Sludge Pyrolysis Pilot Plant. *Catalysts* **2025**, *15*, 142. [CrossRef]
26. Mirshafiee, F.; Karimzadeh, R. Intelligent Catalyst Shaping: Effect of Binders on the Physicochemical and Catalytic Properties of Zeolite-Based Catalysts. *J. Chem. Pet. Eng.* **2024**, *58*, 131–147. [CrossRef]
27. Zhao, L.; Zhao, Y.; Wang, S.; Yue, H.; Wang, B.; Lv, J.; Ma, X. Hydrogenation of Dimethyl Oxalate Using Extruded Cu/SiO_2 Catalysts: Mechanical Strength and Catalytic Performance. *Ind. Eng. Chem. Res.* **2012**, *51*, 13935–13943. [CrossRef]
28. Gandhi, D.; Bandyopadhyay, R.; Soni, B. Naturally Occurring Bentonite Clay: Structural Augmentation, Characterization and Application as Catalyst. *Mater. Today Proc.* **2022**, *57*, 194–201. [CrossRef]
29. Moreno de la Calle, Á.; Megía, P.J.; Calles, J.A.; Carrero, A.; Vizcaíno, A.J. Shaped Mesostructured Ni/CeO_2 as Active Catalysts in Hydrogen Production from Acetic Acid Oxidative Steam Reforming. *Int. J. Hydrogen Energy* **2026**, *223*, 154301. [CrossRef]
30. Martínez, M.; Megía, P.J.; Sánchez, N.; de la Calle, A.M.; Carrero, A.; Salazar, A. Co-Cr/SBA-15 Shaped Catalysts: Structural Integrity and Catalytic Performance for Hydrogen Production via Methanol Autothermal Reforming. *Chem. Eng. Res. Des.* **2026**, *233*, 669–680. [CrossRef]
31. Yildiz, R.; Dhainaut, J.; Ciotonea, C.; Dacquin, J.P.; Royer, S.; Courtois, C.; Lorgouilloux, Y. Improving Mechanical Stability of SBA-15 Monoliths Prepared from Polymeric Scaffolds Replication Using Bentonite Clay. *J. Porous Mater.* **2025**, *32*, 1561–1569. [CrossRef]
32. Vajglová, Z.; Kumar, N.; Peurla, M.; Peltonen, J.; Heinmaa, I.; Murzin, D.Y. Synthesis and Physicochemical Characterization of Beta Zeolite–Bentonite Composite Materials for Shaped Catalysts. *Catal. Sci. Technol.* **2018**, *8*, 6150–6162. [CrossRef]
33. Chen, J.; Zhang, X.; Arandiyan, H.; Peng, Y.; Chang, H.; Li, J. Low Temperature Complete Combustion of Methane over Cobalt Chromium Oxides Catalysts. *Catal. Today* **2013**, *201*, 12–18. [CrossRef]
34. Yun, D.; Baek, J.; Choi, Y.; Kim, W.; Lee, H.J.; Yi, J. Promotional Effect of Ni on a CrO_x Catalyst Supported on Silica in the Oxidative Dehydrogenation of Propane with CO_2. *ChemCatChem* **2012**, *4*, 1952–1959. [CrossRef]
35. Li, X.; Li, S.; Cheng, Y.; Zheng, L.; Song, L.; Zi, X.; Dai, H. The Activation of Oxygen Species on the Pt/CeO_2 Catalyst by H_2 for NO Oxidation. *Catalysts* **2024**, *14*, 778. [CrossRef]
36. Megía, P.J.; Morales, A.; Vizcaíno, A.J.; Calles, J.A.; Carrero, A. Oxidative Steam Reforming of Acetic Acid on Ni Catalysts: Influence of the La Promotion on Mesostructured Supports. *Int. J. Hydrogen Energy* **2024**, *52*, 1136–1145. [CrossRef]

37. Megía, P.J.; Rocha, C.; Vizcaíno, A.J.; Carrero, A.; Calles, J.A.; Madeira, L.M.; Soria, M.A. Thermodynamic Comparison between Conventional, Autothermal, and Sorption-Enhanced Bio-Oil Steam Reforming. *Energy Fuels* **2025**, *39*, 1652–1667. [CrossRef]
38. Meshksar, M.; Farsi, M.; Rahimpour, M.R. Hydrogen Production by Steam Reforming of Methane over Hollow, Bulk, and Co-Precipitated Ni–Ce–Al_2O_3 Catalysts: Optimization via Design of Experiments. *J. Energy Inst.* **2023**, *110*, 101344. [CrossRef]
39. Putra, I.D.; Maitarad, P.; Yokoya, M.; Ei, Z.Z.; Hotta, D.; Shi, L.; Rungrotmongkol, T.; Chanvorachote, P. QSAR Machine Learning-Guided Discovery of Renieramycin Right-Half Derivatives with Cytotoxic Activity against NSCLC Cells. *Sci. Rep.* **2025**, *15*, 43516. [CrossRef]
40. Agwu, O.E.; Alatefi, S.; Alkouh, A. Modelling the Future of Cleaner Energy: Explainable Artificial Intelligence Model for Green Hydrogen Production Rate Estimation. *Clean. Eng. Technol.* **2025**, *27*, 101040. [CrossRef]
41. Koltsakidis, S.; Koidi, V.; Lappas, A.; Heracleous, E.; Tzetzis, D. Influence of Binder Concentration in Zeolitic ZSM-5/Bentonite 3D-Printed Monoliths Manufactured through Robocasting for Catalytic Applications. *Int. J. Adv. Manuf. Technol.* **2023**, *126*, 259–271. [CrossRef]

Disclaimer/Publisher's Note: The statements, opinions and data contained in all publications are solely those of the individual author(s) and contributor(s) and not of MDPI and/or the editor(s). MDPI and/or the editor(s) disclaim responsibility for any injury to people or property resulting from any ideas, methods, instructions or products referred to in the content.